Electronic Supplementary Information

Synthesis of Titanates for Photomineralization of Industrial Wastewater and Organic pollutants

Ramesh Gade,[a#] Manohar Basude,[a] Narendra Babu Simhachalam,[b] Vummadi Ramadevi,[c] Someshwar Pola[a]* and Prabhakar Chetti[d]*

[a] Material Research lab, Department of Chemistry, Osmania University, Hyderabad, India
[b] Department of Physics, Osmania University, Hyderabad, India
[c] Chaitanya Bharathi Institute of Technology, Hyderabad, India
[d] Department of Chemistry, National Institute of Technology, Kurukshetra, India
[#] current address: *Department of Humanities & Sciences, Vardhaman College of Engineering, Hyderabad, Indi*a

Experimental techniques

The SEM images were acquired utilising an HITACHI SU-1500 variable pressure scanning electron microscope (VP-SEM). For phase confirmation, room-temperature X-ray diffractograms of all materials were acquired using a Rigaku miniplex powder X-ray diffractometer (Cu Kα, ë = 1.5406 Å) in the 2θ range 0 - 80º. FEI TECNAI G2S-Twin transmission electron microscope was used to measure TEM (transmission electron microscopy) pictures (Model no: 02083). The X-ray photoelectron spectroscopy (XPS) measurements were carried out on a KRATOS AXIS165 X-ray photoelectron spectrometer with excitation energy of 1253.6 eV (Mg Ka) and passed energy of 80 eV. Using a Shimadzu differential thermal analyzer (DTG-60H) with a heating rate of 10°C/min in the range from 50 °C to 1000 °C and a Nitrogen purging rate of 20 mL/min, thermograms of all samples were acquired. By measuring nitrogen adsorption-desorption isotherm measurements at 77 K with a Quantachromeautosorb automated gas sorption system, Brunauer-Emmett-Teller (BET) surface areas were estimated. All photoreactions were conducted utilising a multi-tube photoreactor system with visible tungsten light, manufactured by Lelesil Innovative Systems in India. On a JASCO V-760 UV-vis spectrophotometer, UV-visible DRS spectra were acquired. On a Cary Eclipse Fluorescence Spectrophotometer, the photoluminescence (PL) spectra of the catalysts were recorded while the samples were excited at their respective absorption maxima. Current density was measured using a typical three-electrode system and an electrochemical workstation (CHI 660). A flexible Fluorine-doped tin

oxide (FTO) substrate (1 cm × 1 cm) covered with the catalyst, acts as the working electrode. A platinum wire and Ag/AgCl were used as the counter and reference electrodes respectively, with 0.05 M K_2SO_4 solution as the electrolyte.

1.Preparation of Ag-loaded $PdTi_3O_7$ Nanoparticles

Step-1: Ion-exchange-ultrasonication technique for preparation of $PdTi_3O_7$

The starting material, $Na_2Ti_3O_7$ (**NaTO**)[1], was subjected to ultrasonication for two hours in a solution of $Pd(NO_3)_2$ to form $PdTi_3O_7$ (**PdTO**). Typically, 1 g of **NaTO** powder was ultrasonicated in 100 mL of 0.1 M $Pd(NO_3)_2$ solution at room temperature. The color of the powder changed from colorless to dark brown, and the ultrasonication continued for 2 hours to assure completion of ion-exchange. The solid materials were separated by filtration, and the remaining solution was checked for Pd^{2+} ion by complexometric titration method [2] to ensure the completion of ion exchange process. The solid materials were washed thoroughly with de-ionized water and dried at 200 °C for 3 hours.

Step-2: 1g of **PdTO** was suspended in an aqueous solution containing ethanol (10 % V/V) and 1M $AgNO_3$, and then stirred and ultrasonicated for 2 hours. The Ag-loaded **PdTO** particles were filtered and thoroughly washed with de-ionized water and dried at 150 °C for 3 hours.

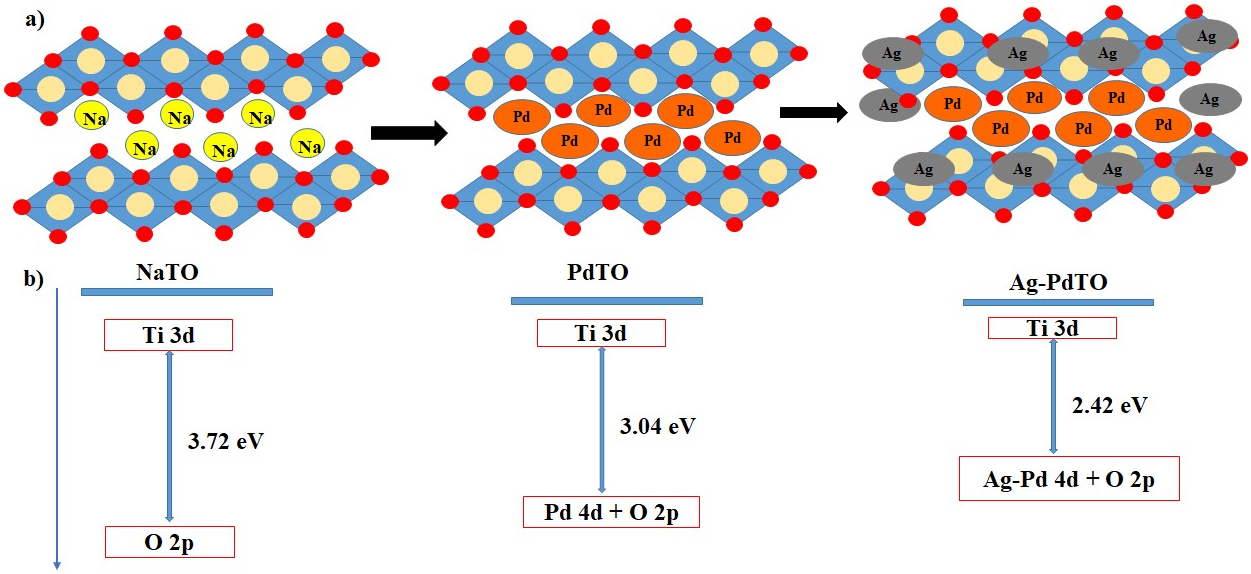

Figure S1 a) Model tunnel structures of NaTO, PdTO and Ag-PdTO (yellow, brownish orange, gray balls represent Na^+, Pd^{2+} and Ag NPs) and b) Projected energy diagrams of NaTO, PdTO and Ag/PdTO.

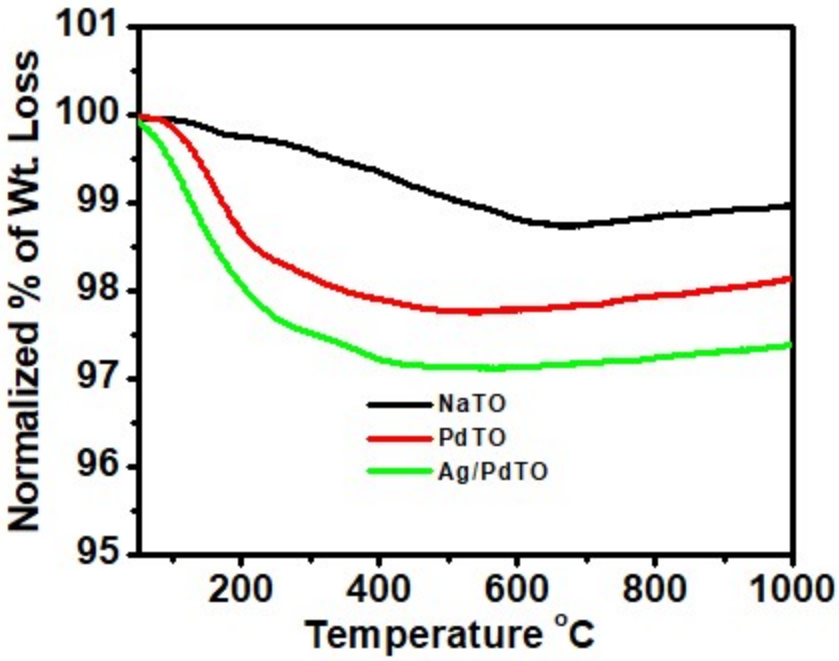

Figure S2 Thermograms of NaTO, PdTO and Ag/PdTO

We have conducted an XRF-Gun (SPECTRO xSORT handheld X-ray fluorescence (XRF) spectrometer) experiment with 1:10 ratio of Ag/PdTO] and Starch powder to know the composition of Ag/PdTO material and the value of Ag is 0.47 g. It is also cross verified with ICP-OES experiment, the amount of Ag is 0.49 g., Tables S1 and Figure S3. The variation among the ICP-OES and the XRF of the Ag nanoparticles of the catalyst prepared by ultrasonication method was almost same, which designated that the prepared Ag/PdTO catalyst is almost 3 mol % Ag nanoparticles.

Table S1 Amount of Ag nanoparticles formed on PdTO from ICP-OES and XRF analysis

Element	ICP-OES (mg) per 1.0 g of Ag/PdTO	XRF (mg) per 1.0 g of Ag/PdTO
Ag	0.49	0.47

Method: Mining-H | PP4 8/17/2022 7:47:13 AM

Name: agpdto

Description: 2

Duration of measurement: 60.1 s (40.0/20.1)

Symbol	Si / %	P / %	S / %	Cl / %	K / %	Ca / %	Ti / %	Fe / %
Conc.	.079	.042	.007	.054	0.12	.081	7.02	.013
U	± .009	± .004	± .002	± .004	± 0.01	± .002	± 0.03	± .001

Symbol	Co / %	Ni / %	Zn / %	Se / %	Sr / %	Y / %	Zr / %	Ag / %
Conc.	.002	.001	.002	.002	.001	.001	.006	0.47
U	± .001	± .001	± .001	± .001	± .001	± .001	± .001	± 0.01

Symbol	In / %	I / %	Cs / %	W / %	Hg / %	Tl / %	Pb / %	Bi / %
Conc.	.042	.026	.009	.003	.003	.002	.001	.001
U	± .001	± .002	± .003	± .001	± .001	± .001	± .001	± .001

Symbol	U / %							
Conc.	.002							
U	± .001							

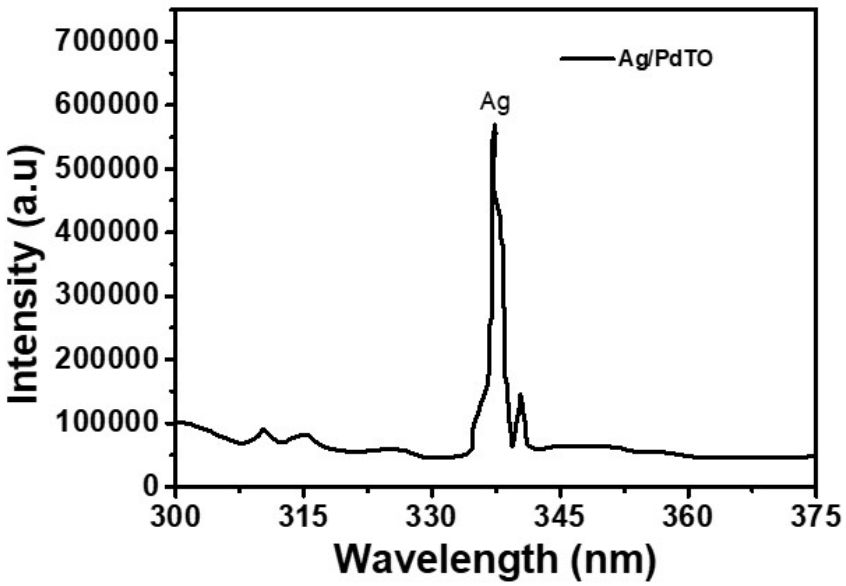

Figure S3 ICP-OES spectrum of Ag Nanoparticles

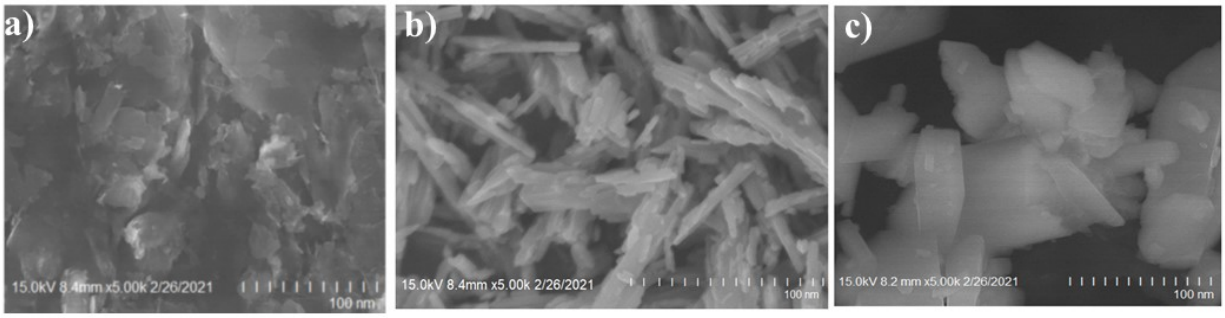

Figure S4 FESEM images of a) NaTO, b) PdTO and c) Ag/PdTO

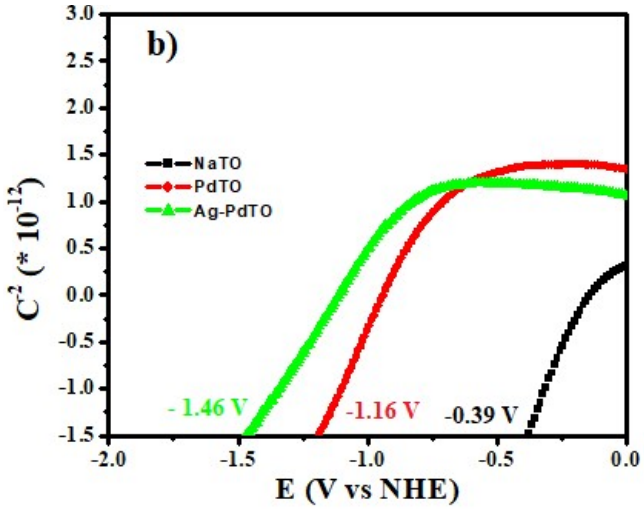

Figure S5 Flat-band potentials of NaTO, PdTO and Ag/PdTO photocatalysts

2. Reflectance and Transmittance Estimations

Aqueous suspensions of the catalysts NaTO, PdTO, and Ag/PdTO were prepared employing different catalyst loads at pH 4: 100, 250, 500, 1000, and 2000 mg/L. Estimations of paralleled diffuse reflectance (DR_λ), transmittance (T_λ), and diffuse transmittance (DT_λ) of these particles-dispersed solutions were carried out with an JASCO V-760 UV-vis spectrophotometer, measuring each 20 nm in the wavelength range from 200 to 600 nm. For every catalyst batch and each wavelength, estimations were examined twice. A flow cell with a pump that circulates the catalyst heterogeneous solution from a tank equipped with a mechanical stirrer was utilized, ignoring the deposition of the catalysts and retain a continual catalyst batch in the estimating cell. The rate of flow and mechanical stirring were cautiously calibrated to confirm

the catalyst batch value and the reliability of the particle concentration throughout the estimations.

3. Photodegradation of various organic dye pollutants

The catalyst (25 mg, 0.05 mol%) was suspended in an aqueous solution of organic dye pollutants (10^{-4} M, 50 mL) in an 80 mL cylindrical quartz glass reactor. The photodegradation of dye was carried out under visible light (300 Watts tungsten light (40 V), with photon flux of 12000 lumens and intensity of 1,61,200 lux for 60 min. Adsorption-desorption pre-equilibrium of the dye was achieved in the dark for 20 min before irradiation and sampling. Samples were collected every 10 minutes and filtered through a Millipore filter to remove the catalyst particles and then examined by UV-Vis spectrophotometer at respective λmax value. Degradation of anionic dyes such as Methyl Red (MR), Reactive X3B (X3B) and Cotton Blue (CB)) and cationic dyes such as Methylene Blue (MB), Methyl Violet (MV), and Rhodamine B (RhB)) were carried out similarly and monitored at their respective absorption maxima.

3. Degradation of industrial wastewater (IWW)

0.125 g of catalyst was suspended in 500 mL of IWW (obtained from the industrial area near Hyderabad) in a continuous double type cylindrical quartz glass reactor. The photodegradation experiments were performed under visible light with 300 Watts for 60 min, and then the obtained degraded water samples were further exposed to UV-vis irradiation (125 Watts low-pressure mercury lamp (LPML), Techinstro, India) with a photon flux of 3.597×10^8 Einstein/s for 240 min, as reported previously[3]. Dark adsorption tests were carried out for 10 min to attain the adsorption-desorption equilibrium for the visible light process. Whereas for UV-visible light, dark adsorption tests were carried out for 30 min. Samples were collected at every 10 min (visible light) and 30 min (UV-Vis light) and analyzed with a UV-Vis spectrophotometer up to 800 nm.

4. Incineration of Solid-waste

The solid-waste was separated from IWW using the specially designed system and incinerated at 600 ^oC under high vacuum (10^{-5} Torr) to give black-colored ash. The obtained ash was characterized by powder XRD, FESEM and HRTEM.

5. Mott−Schottky plot (Figure S5) equation

$$\frac{1}{C^2} = \frac{1}{C_H^2} + \frac{2}{\varepsilon_r \varepsilon_0 q A^2 N_D}(U - U_{fb} - \frac{kT}{q})$$

where T is the absolute temperature, k is the Bohr constant, U is the applied potential, U_{fb} is the flatband potential, N_D is the doping density, A is electrode surface area, ε_r is the dielectric constant of the semiconductor, ε_0 is the permittivity of free space, q is the electronic charge, C is the space charge layer capacitance, and C_H is the Helmholtz double-layer capacitance.

6. Reflectance and Transmittance Estimations.

Aqueous suspensions of the catalysts NaTO, PdTO, and Ag/PdTO were prepared employing different catalyst loads at pH 4: 100, 250, 500, 1000, and 2000 mg/L. Parallel measurements of diffuse reflectance (DR_λ), transmittance (T_λ), and diffuse transmittance (DT_λ) of these particles-dispersed solutions were carried out with an JASCO V-760 UV-vis spectrophotometer, measuring each 20 nm in the wavelength range from 200 to 600 nm. For each catalyst batch and each wavelength, estimations were examined twice. A flow cell with a pump that circulates the heterogeneous catalyst solution from a tank equipped with a mechanical stirrer was utilized, ignoring? the deposit of the catalysts and retain a continual catalyst batch in the estimating cell. The rate of flow and mechanical stirring were cautiously calibrated to confirm the catalyst batch value and the reliability of the particle concentration throughout the estimations.

7. Procedure for Optical Activates Measurements.

The optical activates of new nanomaterials were attained improving the reporting technique earlier described[4]. The RTE can be related to a spectrophotometric cell below mentioned presumptions: i) the cell is assumed to be designed by two parallel tubes parted by the cell width, ii) the spectrophotometer collects an approaching absolutely collimated beam of the incident radiation and the radiation field can be considered to show an azimuthal symmetry, and iii) the optical activates of the suspensions is not depends on time and site. With these presumptions the directly used reported RTE equation [5] as follows:

$$\mu \frac{dI_\lambda(x,\mu)}{dx} + \beta_\lambda I_\lambda(x, \mu) = \frac{\sigma_\lambda}{2} \int_{\mu' = -1}^{1} I_\lambda(x, \mu') P(\mu, \mu') d\mu'$$

Satuf et. al. [6] the Henyey and Greenstein (HG) phase function ($P_{HG,\lambda}$) was considered for the radiation typical in the spectrophotometer for reactor cell as follows:

$$P_{HG,\lambda}(\mu_o) = \frac{1 - g_\lambda^2}{(1 + g_\lambda^2 - 2g_\lambda\mu_o)3/2}$$

Where g_λ dimensionless asymmetry factor defined as

$$g_\lambda = \frac{1}{2}\int_{-1}^{1} P_{HG,\lambda}(\mu_o)\,\mu_o d\mu_o$$

Where μ_o is the cosine angle of scattered and incident light.

8. Local volumetric rate of photon absorption (LVRPA) estimation.

The LVRPA is estimated through a spatial distribution of with different photocatalyst lots of Ag/PdTO in a tubular effortlessly stirred reactor with an inner diameter of 15 cm [7] by using the spatial coordinate x. The bottom of the reactor was translucent and irradiated with a cylindrical lamp (visible light with 300 Watts and 125 Watts low-pressure mercury lamp (LPML), Techinstro, India) positioned at the focal axis of a parabolical mirror with a photon flux of 3.597 x 10^{-9} Einstein/cm^2/s as measured through actinometric technique with ammonium tetrathiocyanodiammonochromate (Reinecke salt) [8].

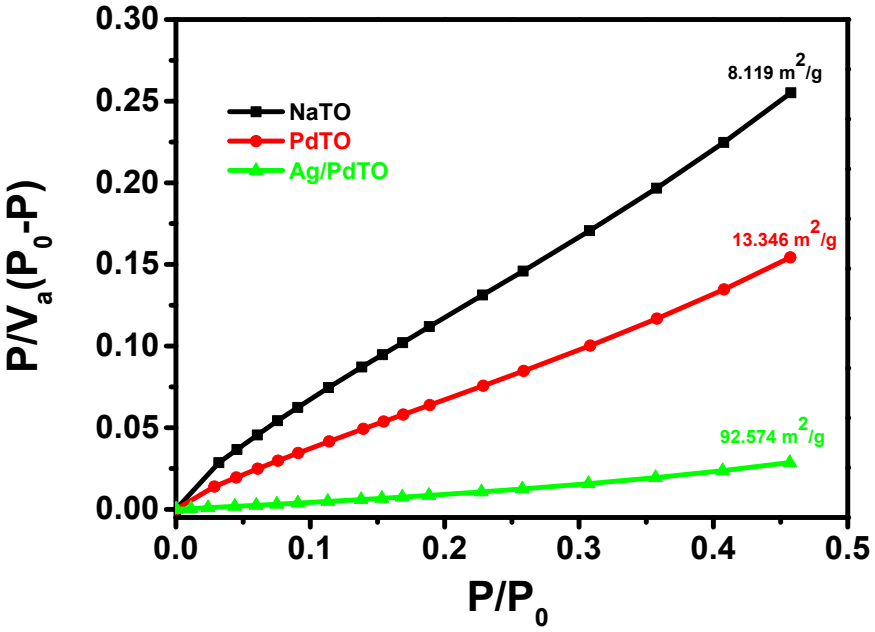

Figure S6 BET surface area plots of NaTO, PdTO and Ag/PdTO materials

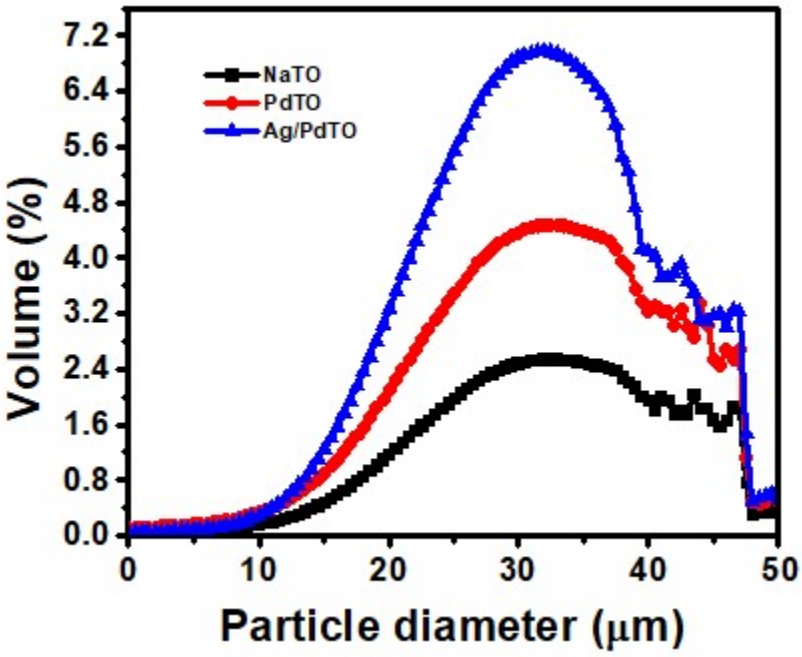

Figure S7 Size distribution of particles for titanates slurries

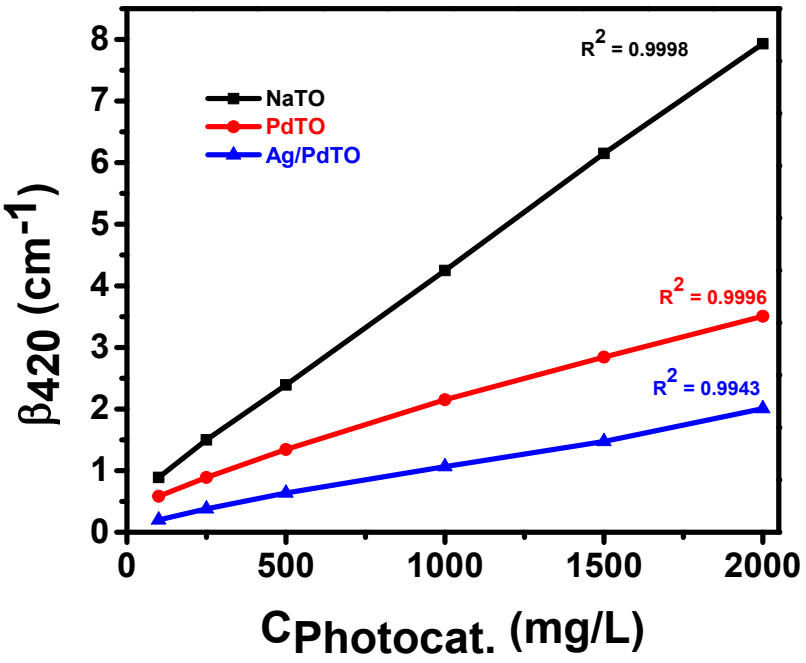

Figure S8 Linear regressions plots among the extinction coefficient and the photocatalyst load at 420 nm for the photocatalysts.

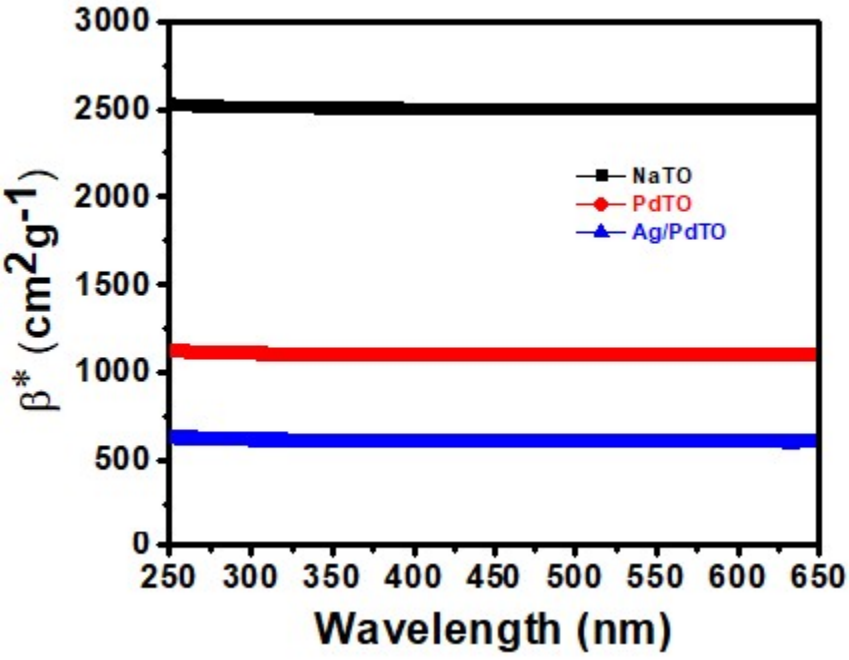

Figure S9 Specific extinction coefficient for the photocatalysts with λ at 420 nm.

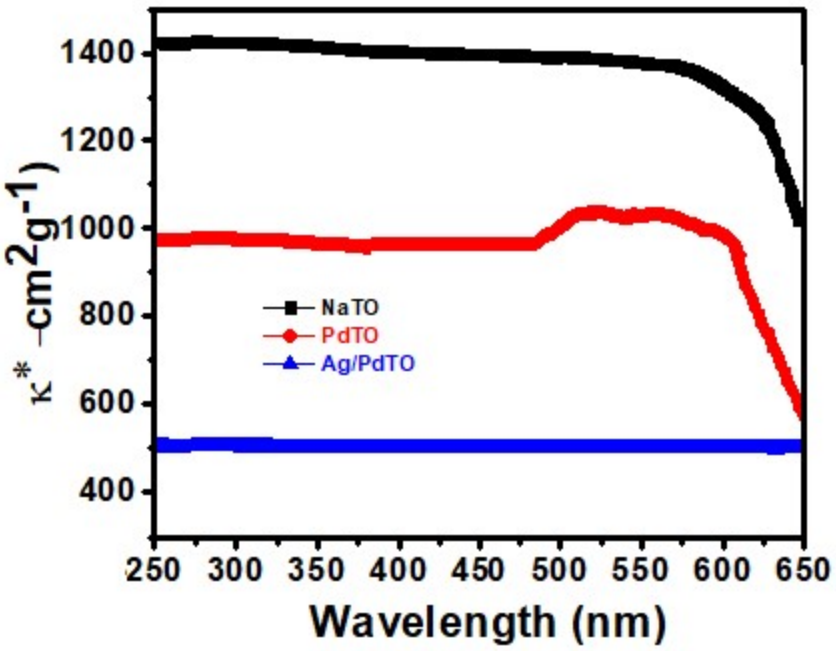

Figure S10 Specific absorption coefficient for the photocatalysts as a function of λ.

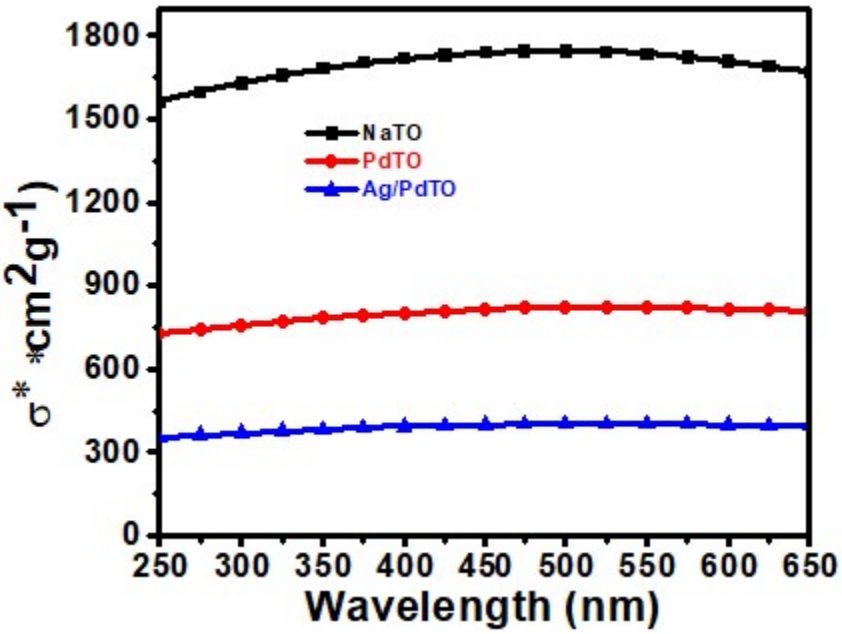

Figure S11 Specific scattering coefficient for the photocatalysts as a function ofλ

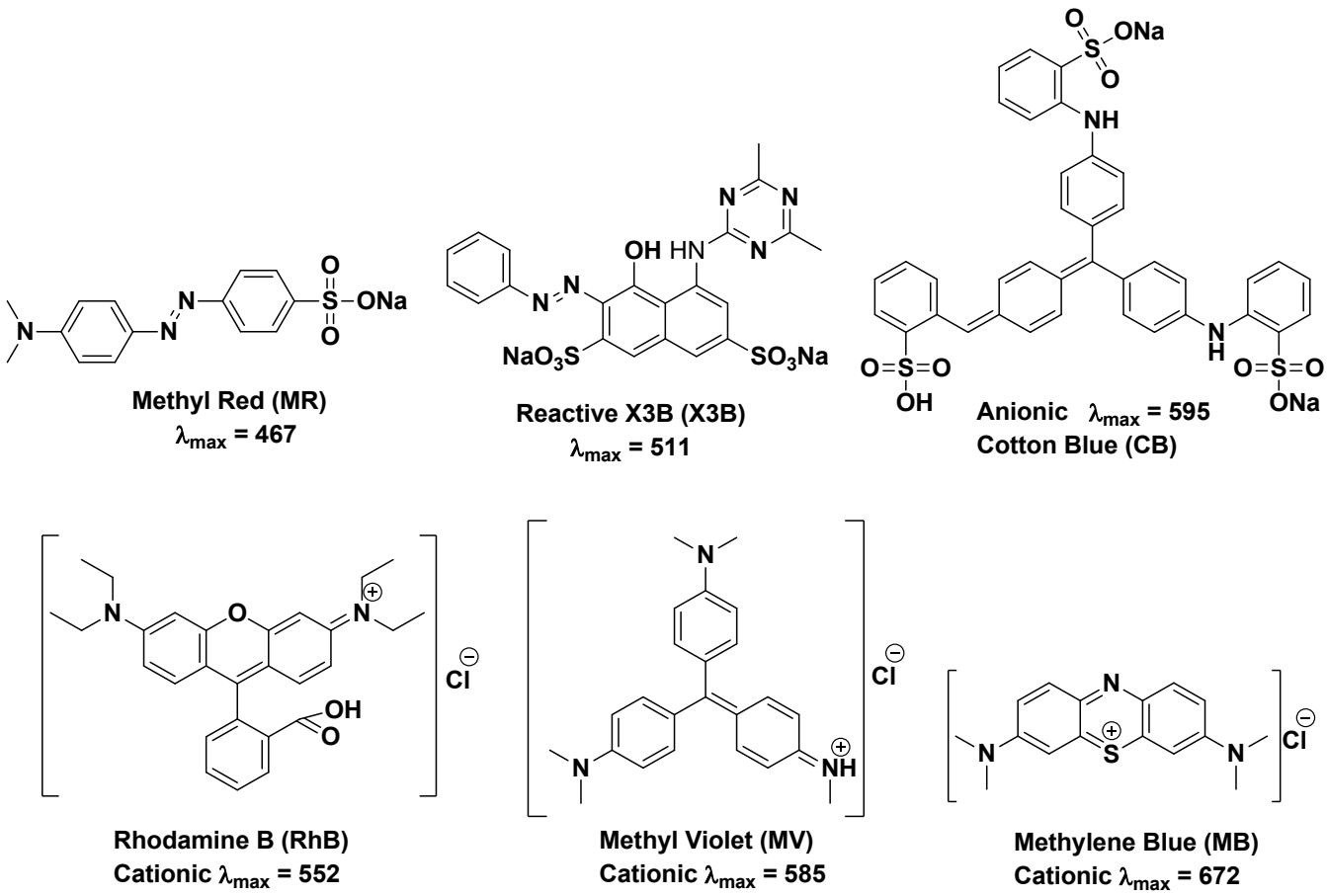

Figure S12 Chemical structures of anionic and cationic dyes used for photodegradation

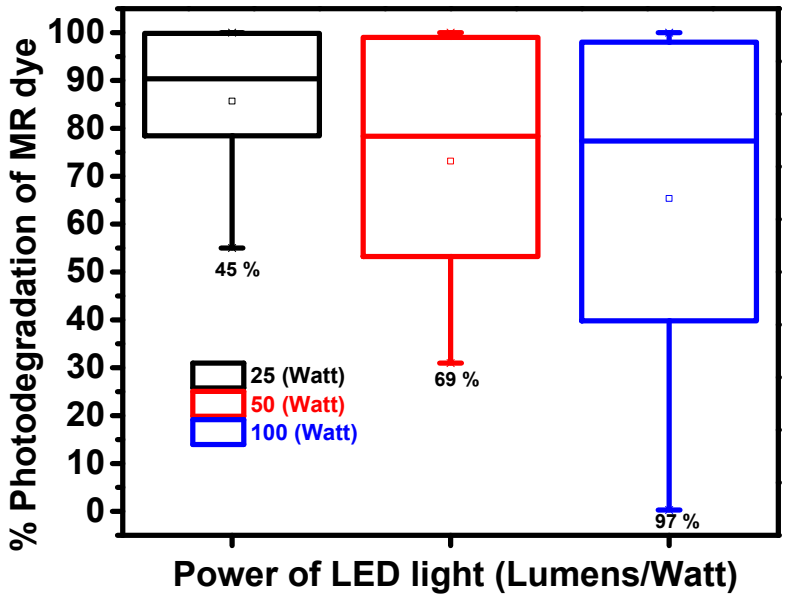

Figure S13 Optimization of power of LED light for photodegradation of MR dye

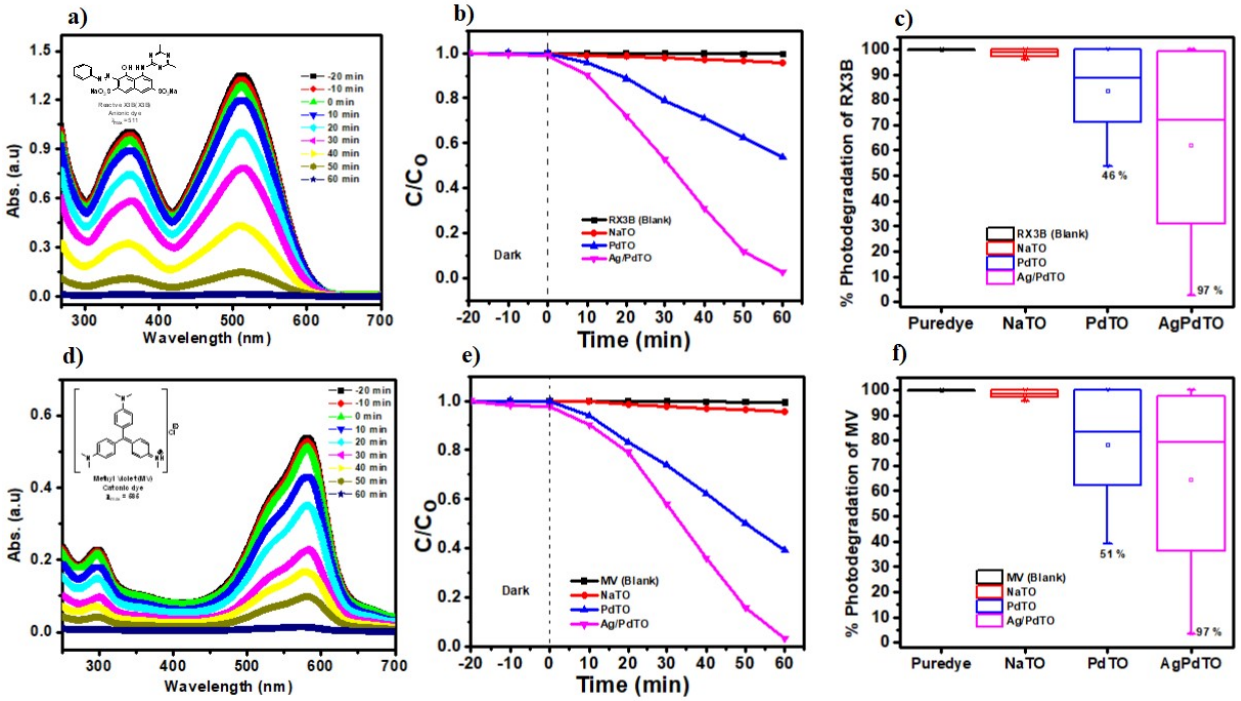

Figure S14 a), d) successive absorbance spectral pattern, b), e) Photodegradation of RX30 and MV and c), f) box chart plot for % of dye degradation in the presence of NaTO, PdTO and Ag/PdTO under visible-light-driven.

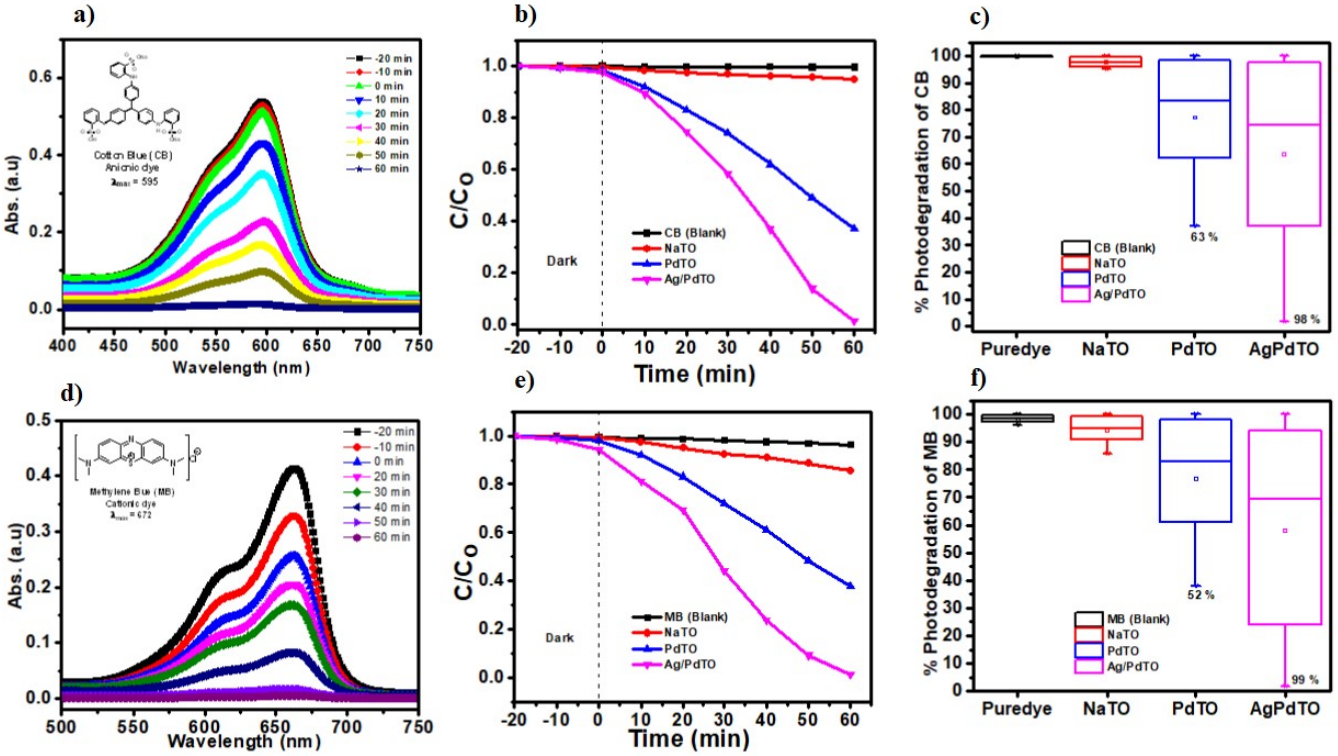

Figure S15 a), d) successive absorbance spectral pattern, b), e) Photodegradation of CB and MB and c), f) box chart plot for % of dye degradation in the presence of NaTO, PdTO and Ag/PdTO under visible-light.

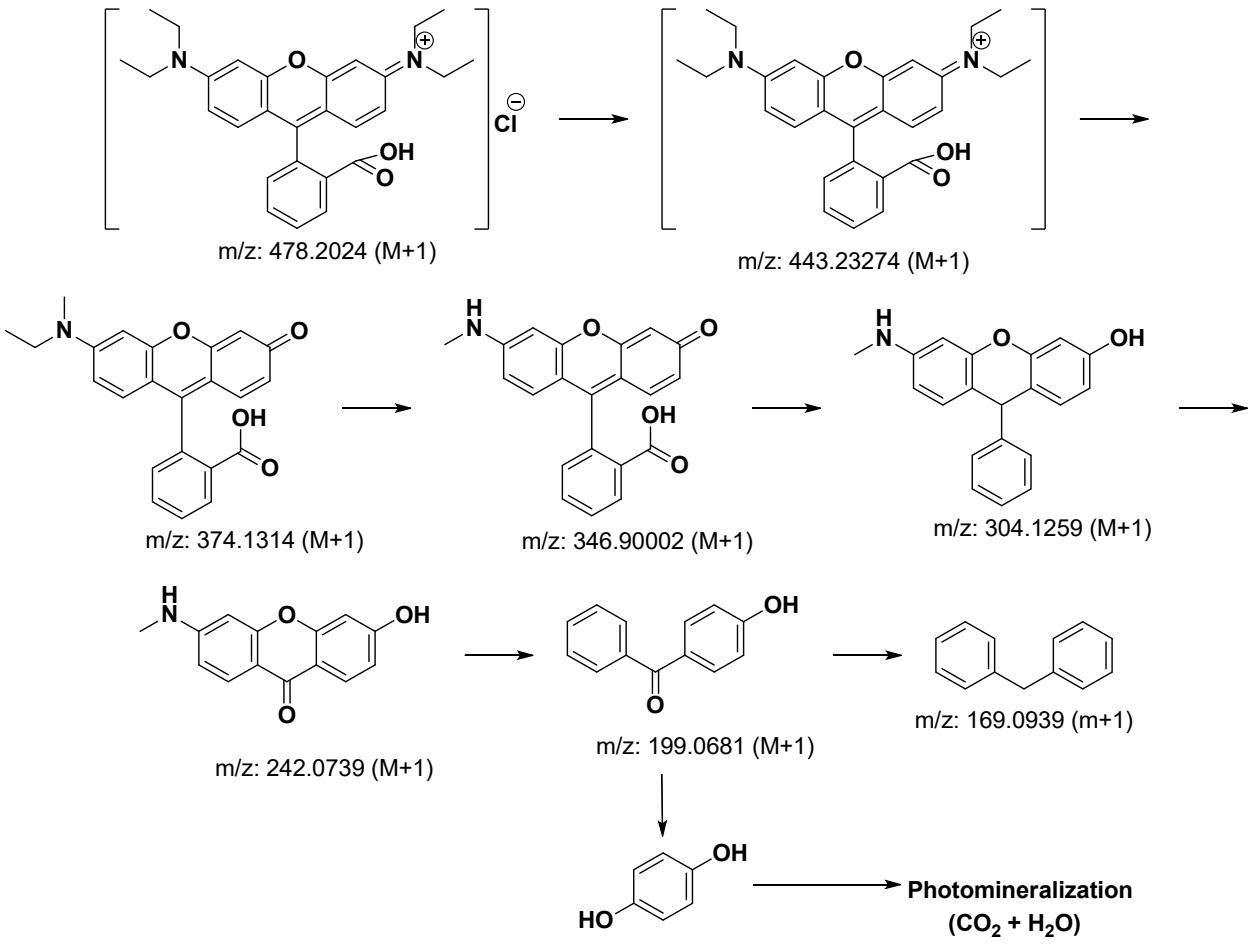

Figure S16 Mass spectral fragmentation pathway for photomineralization of RhB dye

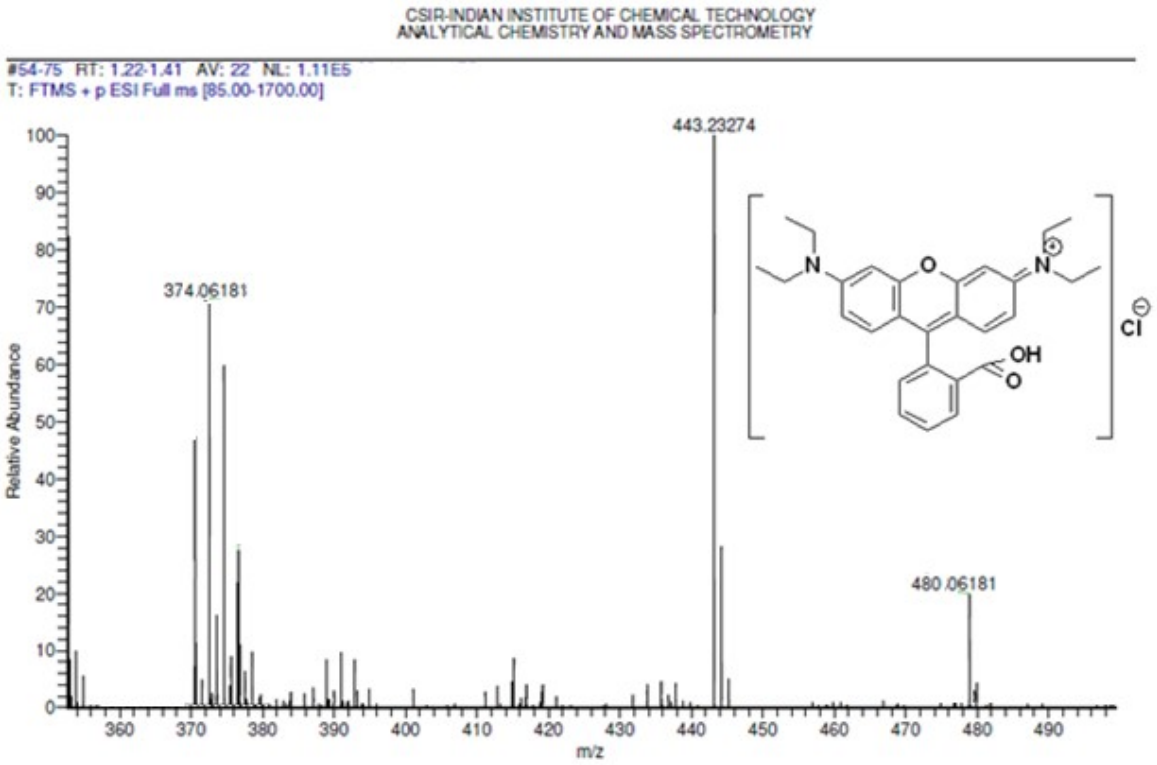

Figure S17a Mass spectra of RhB dye degradation after 10 min under LED light irradiation

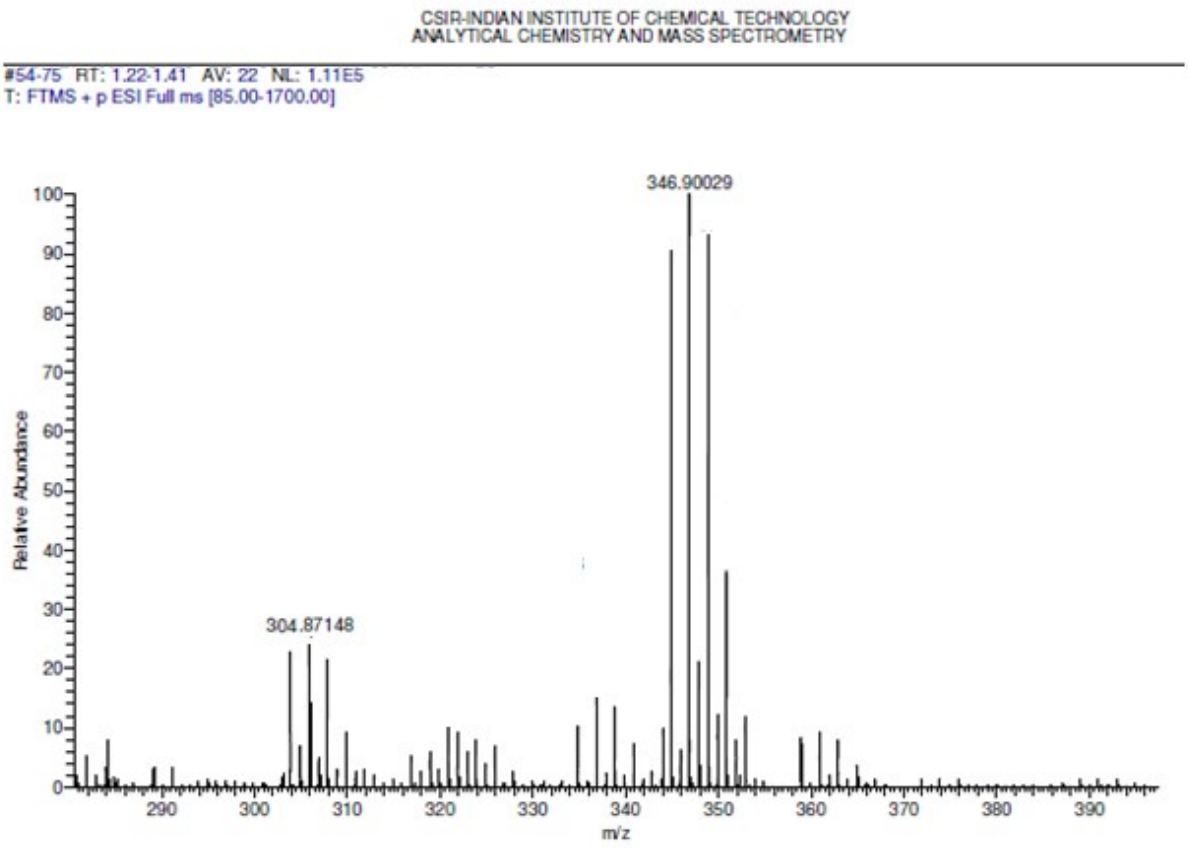

Figure S17b Mass spectra of RhB dye degradation after 20 min under LED light irradiation

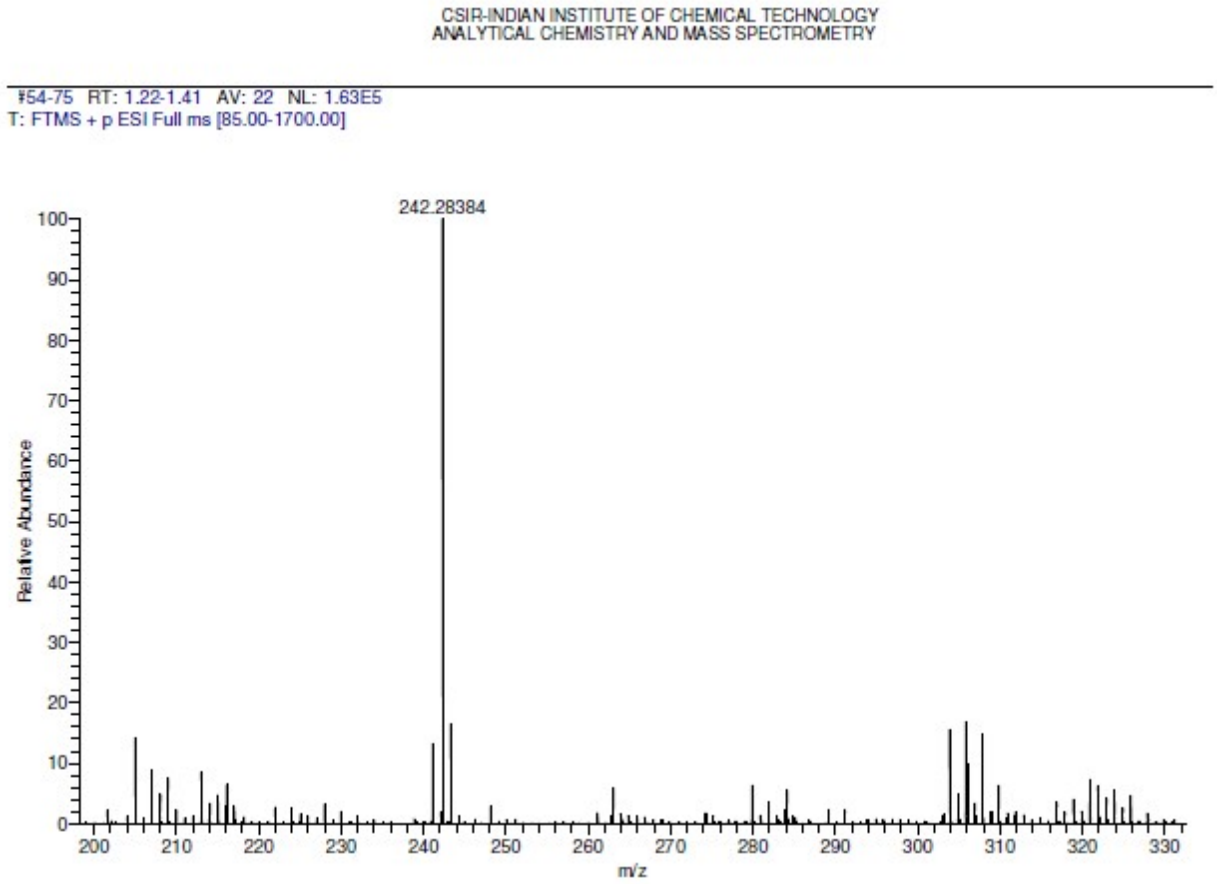

Figure S17c Mass spectra of RhB dye degradation after 40 min under LED light irradiation

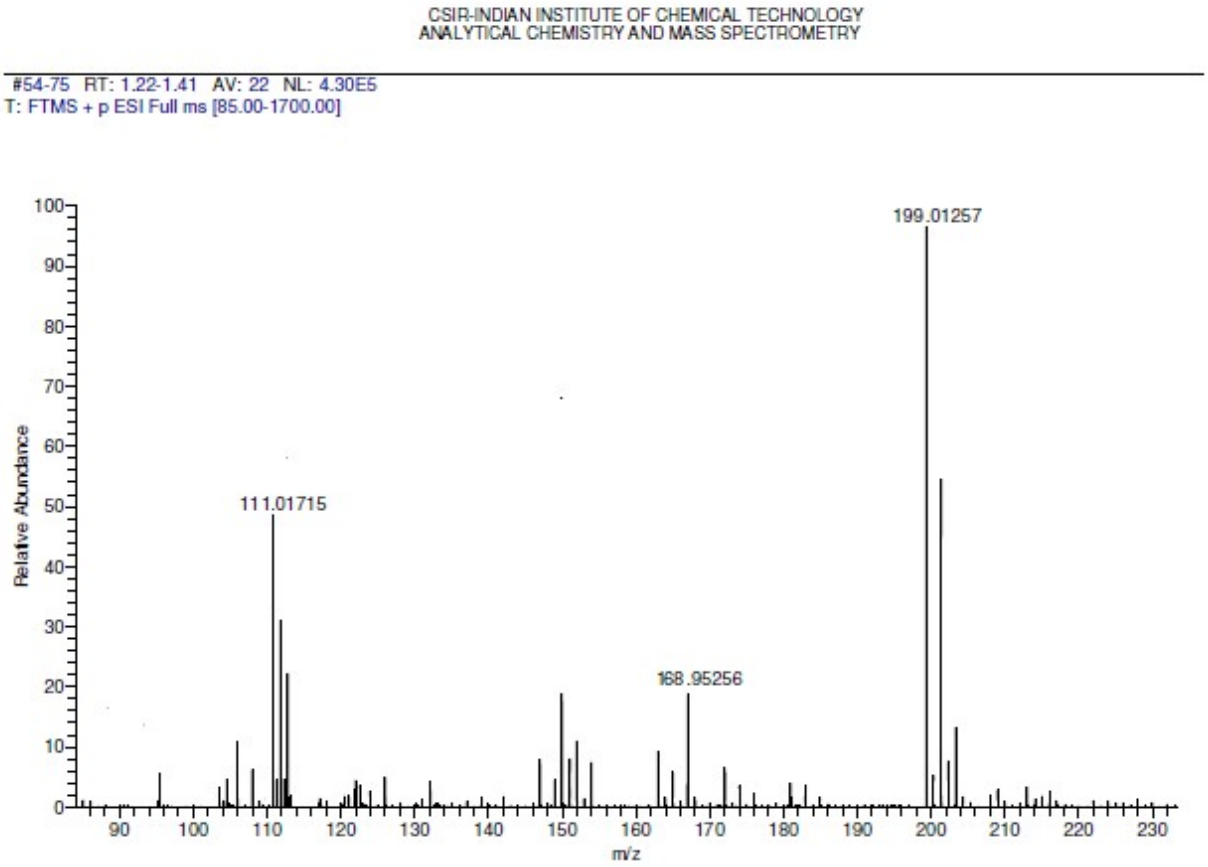

Figure S17d Mass spectra of RhB dye degradation after 50 min under LED light irradiation

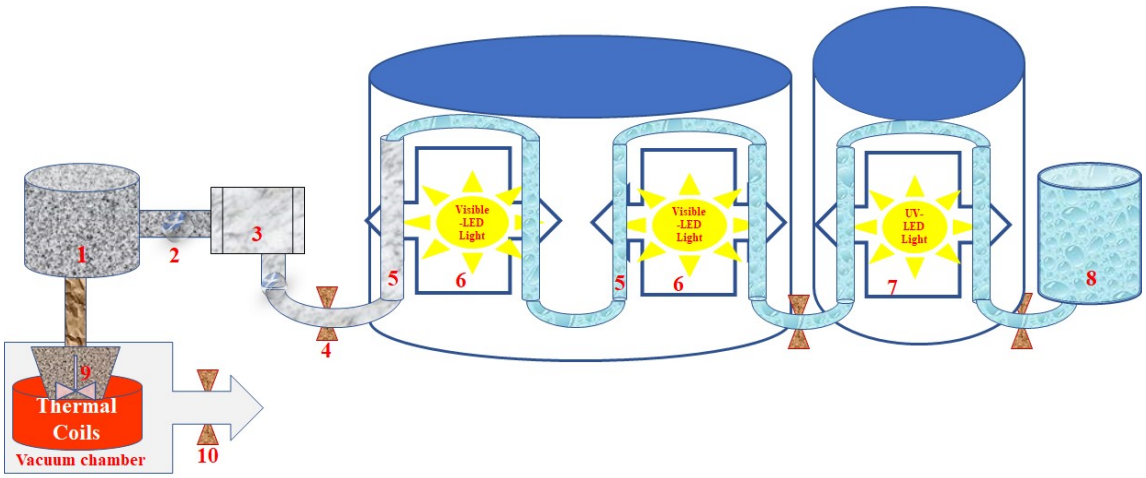

Figure S18 Schematic of Cutting-edge photodegradation process of TPE including 1) effluent tank, 2) macro particles filter, 3) effluent free with macro particles, 4) second micro filter and motor pump, 5) First and second step photodegradation process, 6) LED light,and 7) third-step UV-light-based photodegraded effluent, 8) recyclable water tank (photomineralized water) 9) incineration of solid-waste under high vacuum, and 10) high vacuum trap and valve.

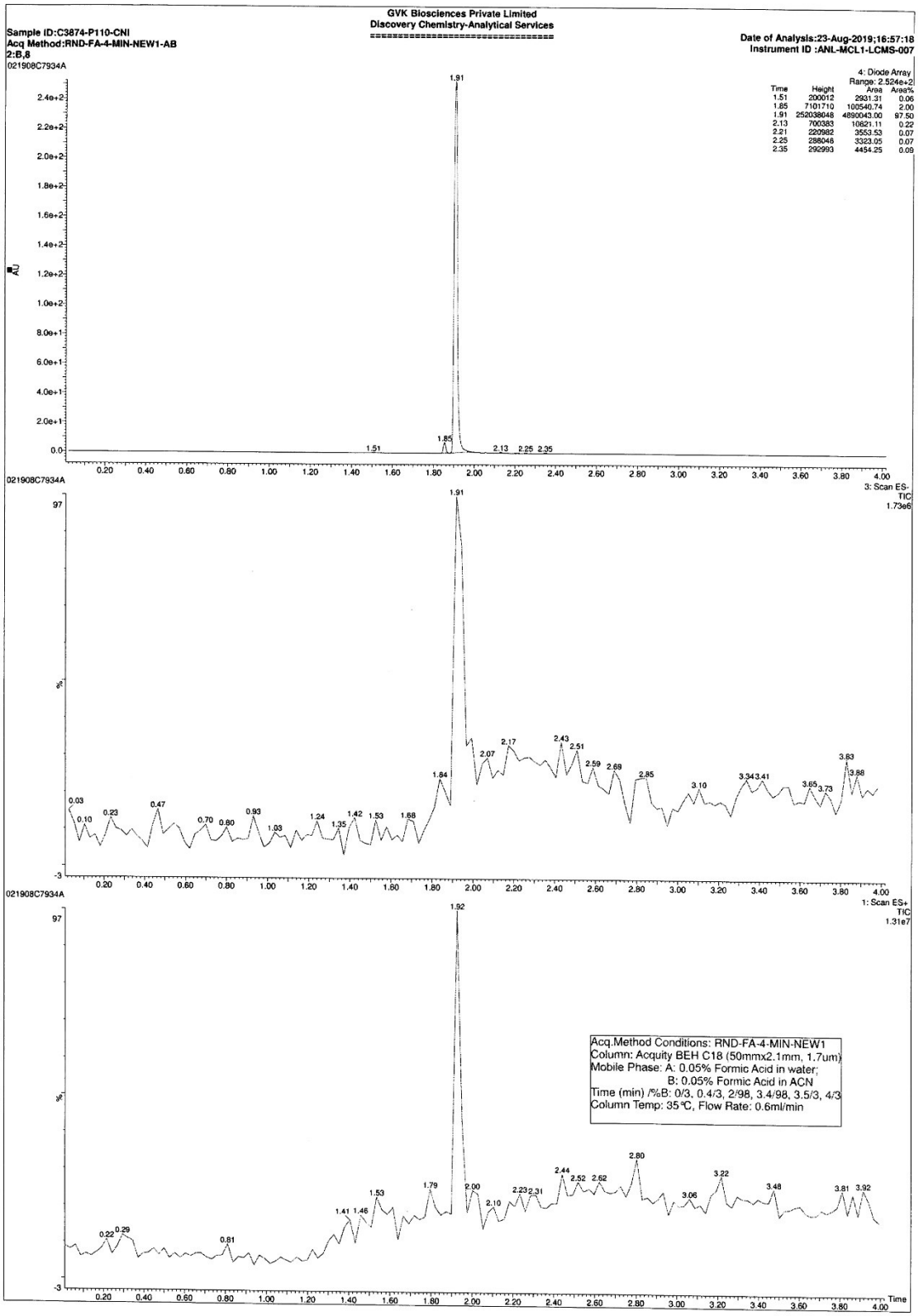

Figure S19a LC pattern of wastewater

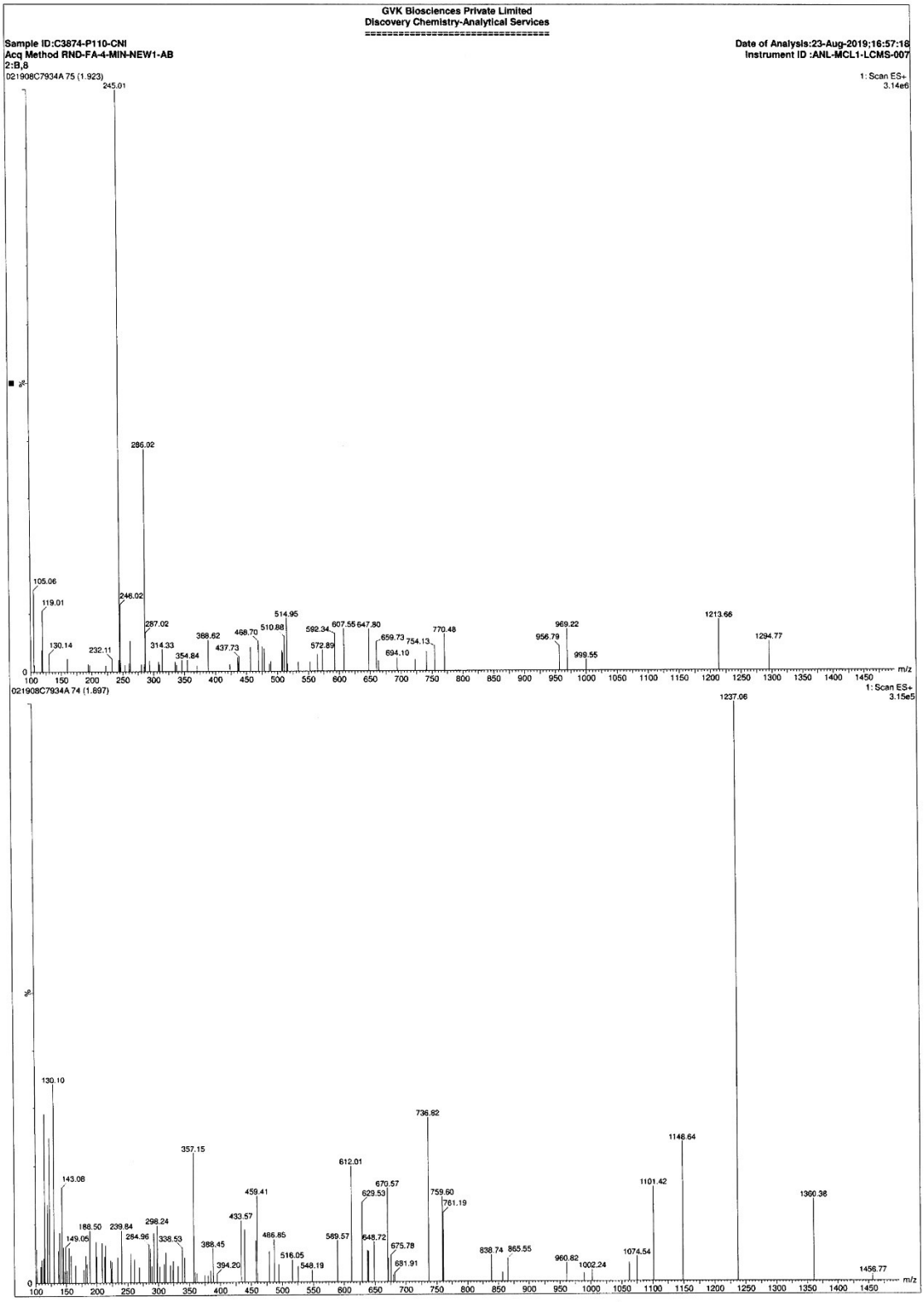

Figure S19b Mass spectra of wastewater

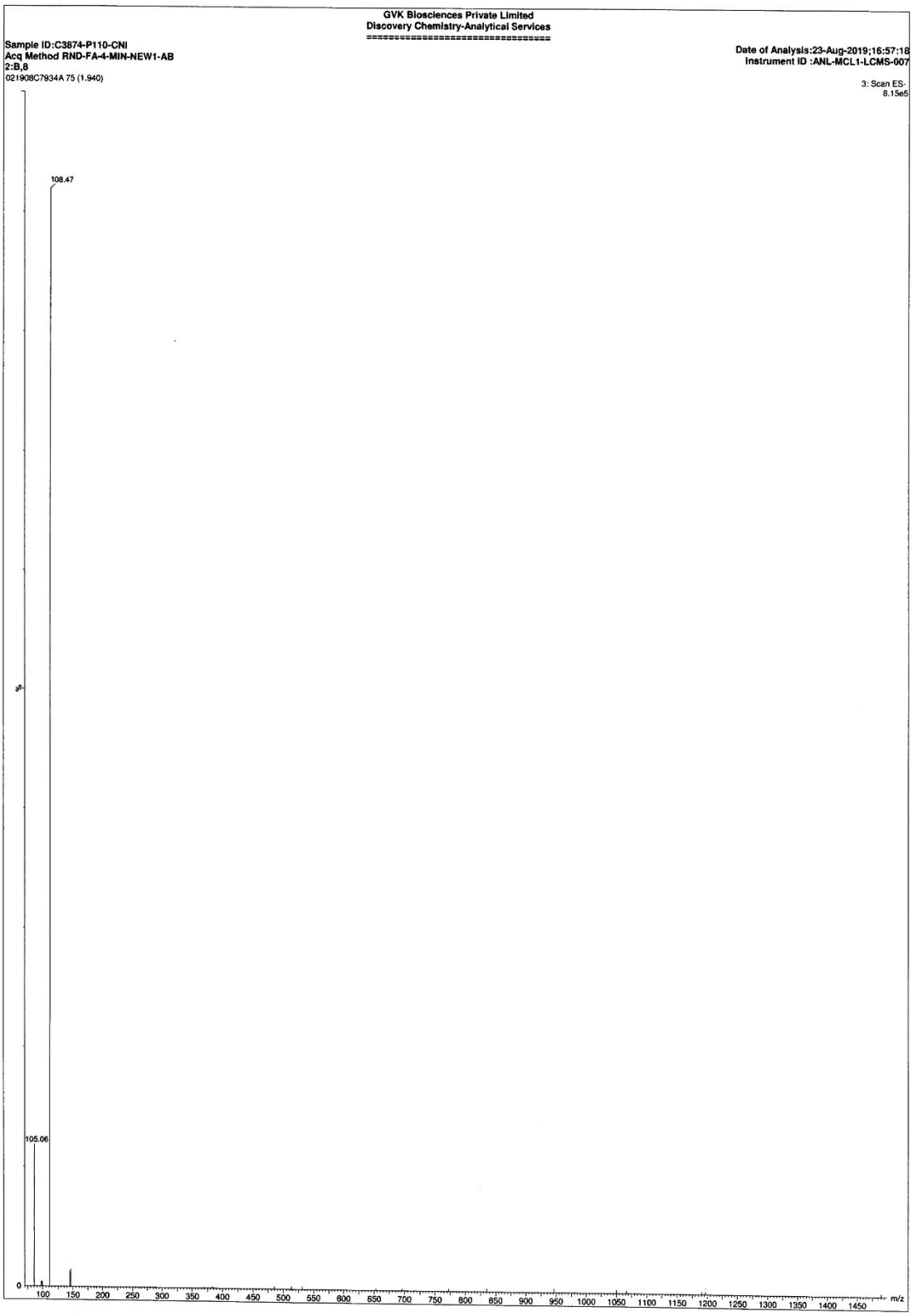

Figure S19c Mass spectra of wastewater after exposed to UV-visible light for 240 min

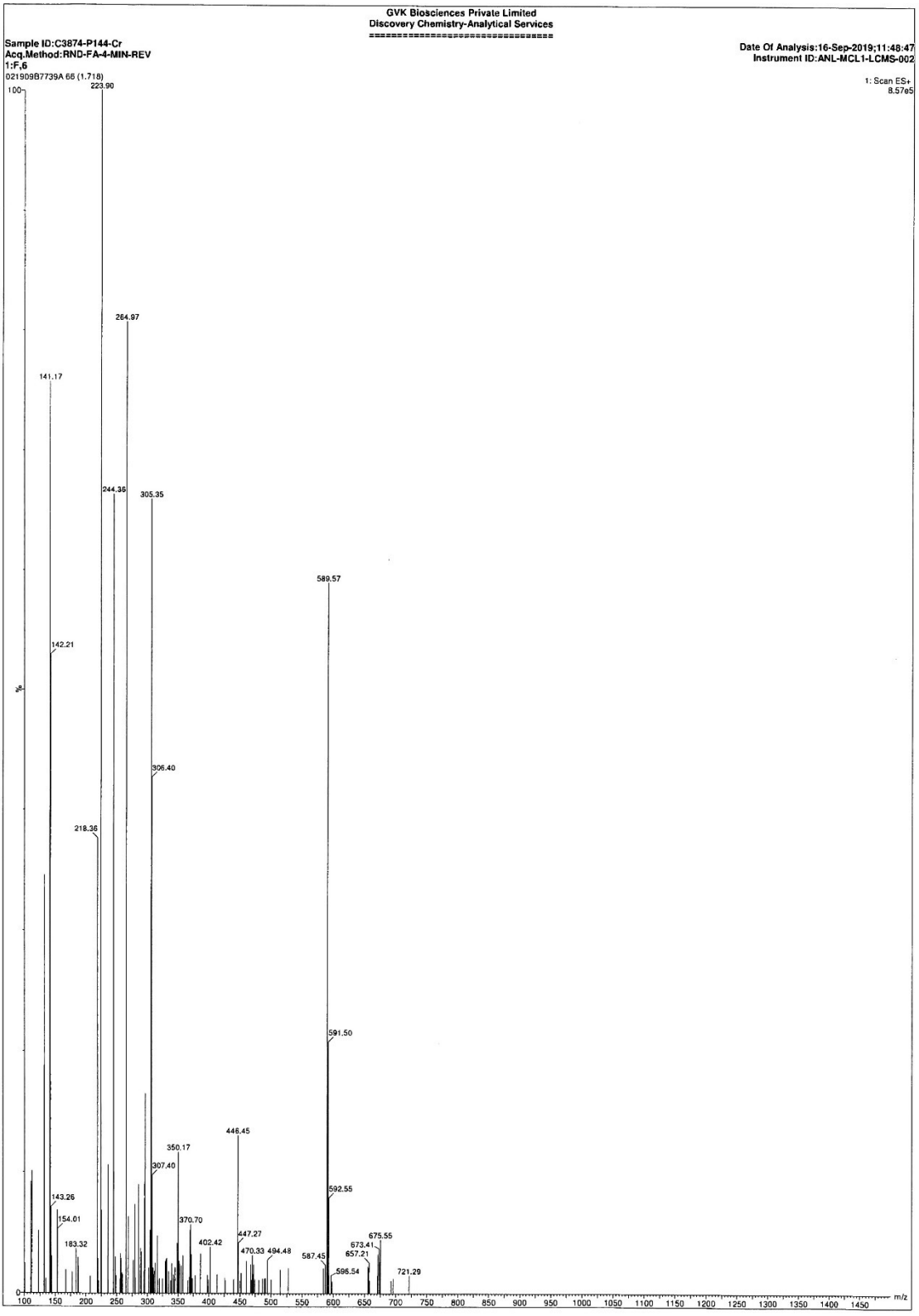

Figure S20 LC-MS data of AIWW sample primary before exposed to visible light irradiation

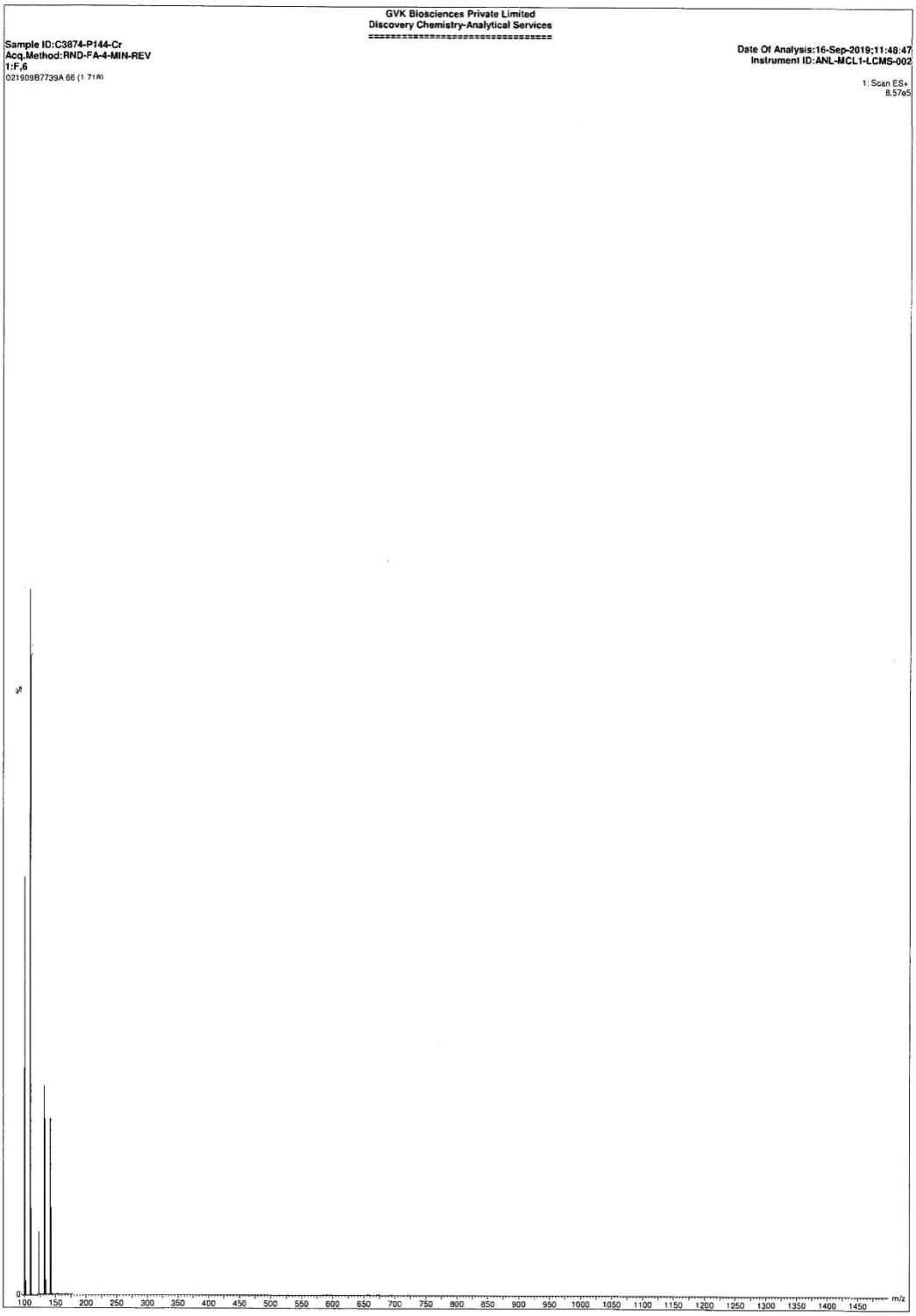

Figure S21 LC-MS data of AIWW sample after 180 min exposed to visible light irradiation

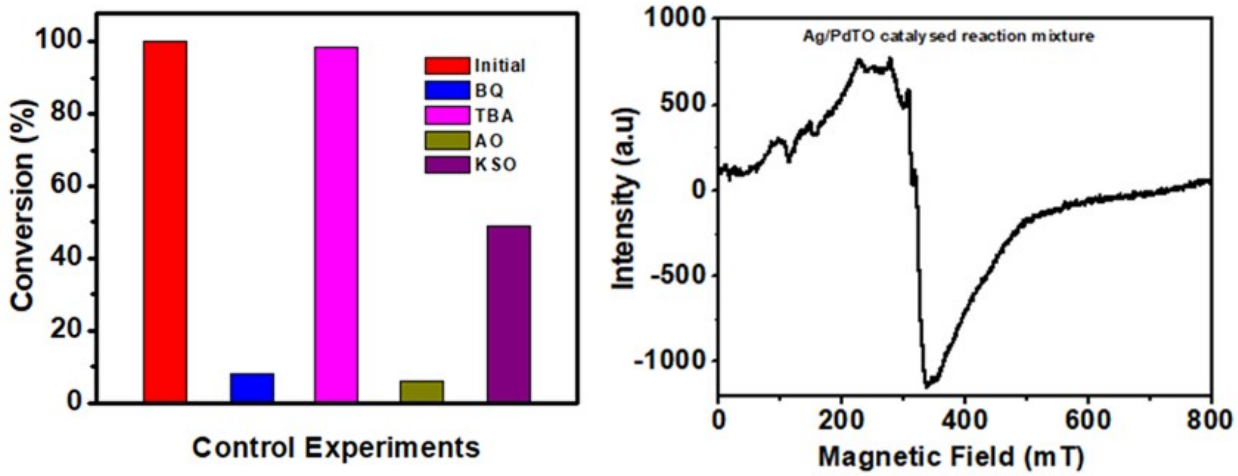

Figure S22 a) Control experiments of selective photooxidation with the adding of several radical scavengers: benzoquinone (BQ, scavenger for superoxide radicals), tert-butyl alcohol (TBA, scavenger for hydroxyl radicals), ammonium oxalate (AO, scavenger for holes) and $K_2S_2O_8$ (KSO scavenger for electrons) over the optimum **Ag/PdTO** under visible light irradiation b) ESR spectra of TPE sample after 20 min. of photodegradation process

General mechanism of photomineralization Process:

The production of $^{\bullet}OH$ / $O_2^{\bullet-}$ radicals in a photoreaction is as follows:

The incident visible light energy is larger or the equal bandgap energy of the Ag/PdTO.

Electrons will be moved from the VB to CB, producing a hole in the VB (equation-1).

Both excited electrons and holes transfer to the surface of the Ag/PdTO and combine with adsorbed O_2 and water to generate $O_2^{\bullet-}$ and $^{\bullet}OH$ radicals respectively (equation-2 and 3).

The H^+ ion responds very fast with $O_2^{\bullet-}$ radicals to form $HO_2^{\bullet}$ (equation-4) species, which interact with one another and form H_2O_2 and O_2 in insitu (equation-5).

Afterward H_2O_2 easily breaks to form $^{\bullet}OH$ radicals (equation-6) that react with dyes or AIWW to progress the mineralization method.

In the case of dye molecules $O_2^{\bullet-}$ radical interacts non-selectively and non-directionally with dyes or AIWW and fragments continuously through a simple mineralization process.

The pathway of mechanism shown as follows:

$$Ag/PdTO + hu \longrightarrow e^-_{cb} + h^+_{vb} \quad (1)$$

$$H_2O + h^+_{vb} \longrightarrow \dot{O}H + H^+ \quad (2)$$

$$O_2 + e^-_{cb} \longrightarrow O_2^{\bullet-} \quad (3)$$

$$O_2^{\bullet-} + H^+ \longrightarrow HO_2^{\bullet} \quad (4)$$

$$2\dot{H}O_2 \longrightarrow H_2O_2 + O_2 \quad (5)$$

$$H_2O_2 \longrightarrow 2HO^{\bullet} \quad (6)$$

$$Dye + \dot{O}H \longrightarrow Mineralization \quad (7)$$

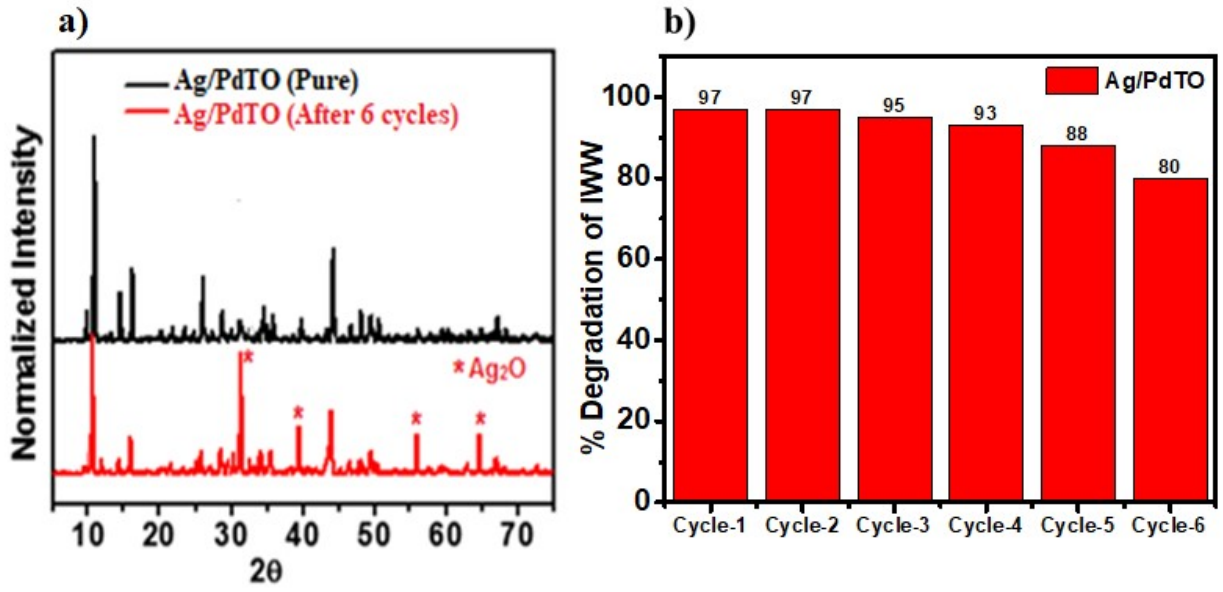

Figure S23 a) P-XRD pattern of Ag/PdTO nanoparticles after six cycles of IWW and b) % of photodegradation process of IWW in the presence of Ag/PdTO repeated six cycles.

Figure S24 High vacuum furnace for incineration of solid-waste obtained from industrial raw wastewater.

Method Name	: CHNS
Method File	: C:\....\Documents and Setting\FlashEA1112\My Documents\NCHS100714\NCHS-100714.mth
Chromatogram	: File1000714-SAMPLE015
Operator ID	: Chung Company Name : IOC, A. Sinica
Analysed	: 2019/12/23 15:54 Printed : 2019/12/23 16:05
Sample ID	: solid-waste
	Instrument N. : Instrument #1
Analysis Type	: UnkNown (Area) Sample weight : 1.456 g

Element Name	Percentage
Carbon	96.9678
Hydrogen	3.0322

Data sheet S1 Elemental analysis of black solid obtained from incineration of solid-waste

NOMENCLATURE

$C_{photocat}$ = photocatalyst load (mg/L)

DR = diffuse reflectance (dimensionless)

g = asymmetry factor (dimensionless)

L = spectrophotometric cell length

LVRPA = local volumetric rate of photon absorption

p = phase function (dimensionless)

S_{BET} = specific surface area determined using the BET model ($m^2\ g^{-1}$)

t = time (s)

T = collimated transmission (dimensionless)

$V_{\mu p}$ = specific micropore volume ($cm^3 g^{-1}$)

V_R = reactor volume (cm^3)

x = axial coordinate (cm)

Symbols

β = volumetric extinction coefficient (cm^{-1})

β_λ* = specific extinction coefficient ($cm^2 g^{-1}$)

δ = Dirac delta function

η = quantum efficiency (dimensionless)

θ = spherical coordinate (rad)

κ = volumetric absorption coefficient (cm^{-1})

κ_λ* = specific absorption coefficient ($cm^2 g^{-1}$)

λ = wavelength (nm)

μ = direction cosine of the ray for which the RTE is written

μ′ = direction cosine of an arbitrary ray before scattering

μ_0 = cosine of the angle between the direction of the incident and the scattered rays

σ = volumetric scattering coefficient (cm^{-1})

σ_λ* = specific scattering coefficient (cm^2g^{-1})

ΔG values for electron transfer processes:

To know the acceptor nature of catalyst Ag/PdTO in mineralization process, we calculated free energy by using Rehm-Weller equation (equation-*a*).

$\Delta G = E_{ox}(D) - E_{red}(A) + C - E^*$ ----------*a*

The oxidation potential of the donor is E_{ox}(D), the reduction potential of the acceptor is E_{red}(A), C is the columbic term and the excitation energy of the fluorescent state is E^*. Then the columbic term in the above expression is neglected[9] due to the nature of solvent is polar, and the neutral species. The calculated ΔG values for the electron transfer processes in the dyes examined in water are negative (Table S2). Therefore, the electron transfer processes were thermodynamically viable.[10]

Table S2: Free energy changes (ΔG) for electron transfer processes between dye and Ag/PdTO catalyst by using Rehm-Weller equation.

Dye	ΔG
Methyl Red	-1.21
Reactive X3B	-1.17
Cotton blue	-1.13
Methylene blue	-1.19
Methyl violet	-1.26
Rhodamine B	-1.09

References:

1. M. Vithal, S. R. Krishna, G. Ravi, S. Palla, R. Velchuri and S. Pola, Synthesis of Cu^{2+} and Ag^+ doped $Na_2Ti_3O_7$ by a facile ion-exchange method as visible-light-driven photocatalysts, *Ceramics International*, 2013, **39**, 8429-8439.

2. B. Lv, G. Zhao, D. Li and C. Liang, Dechlorination and oxidation for waste poly (vinylidene chloride) by hydrothermal catalytic oxidation on Pd/AC catalyst, *Polymer degradation and stability*, 2009, **94**, 1047-1052.
3. W. Xian-Ke, Selective complexometric titration of lead in the presence of large amounts of interfering ions, *Analyst*, 1990, **115**, 1611-1612.
4. G. B. O. de la Plata, O. M. Alfano and A. E. Cassano, Optical properties of goethite catalyst for heterogeneous photo-Fenton reactions: Comparison with a titanium dioxide catalyst, *Chemical Engineering Journal*, 2008, **137**, 396-410.
5. M. A. De Leon, M. Sergio, J. Bussi, G. Ortiz de la Plata, A. E. Cassano and O. M. Alfano, Optical properties of iron pillared clays as catalysts for heterogeneous photo-Fenton process, *Industrial & Engineering Chemistry Research*, 2015, **54**, 1228-1235.
6. M. L. Satuf, R. J. Brandi, A. E. Cassano and O. M. Alfano, Experimental method to evaluate the optical properties of aqueous titanium dioxide suspensions, *Industrial & engineering chemistry research*, 2005, **44**, 6643-6649.
7. G. B. O. de la Plata, O. M. Alfano and A. E. Cassano, Decomposition of 2-chlorophenol employing goethite as Fenton catalyst. I. Proposal of a feasible, combined reaction scheme of heterogeneous and homogeneous reactions, *Applied Catalysis B: Environmental*, 2010, **95**, 1-13.
8. H. Kuhn, S. Braslavsky and R. Schmidt, Chemical actinometry (IUPAC technical report), *Pure and Applied Chemistry*, 2004, **76**, 2105-2146.
9. S. Parret, F. M. Savary, J. P. Fouassier and P. Ramamurthy, Spinorbit-coupling-induced triplet formation of triphenylpyrylium ion: a flash photolysis study, *Journal of Photochemistry and Photobiology A*, 1994, **83**, 205–209.
10. S. Nath, H. Pal, D. K. Palit, A. V. Sapre and J. P.Mittal, Steady-state and time-resolved studies on photoinduced interaction of phenothiazine and 10-methylphenothiazine with chloroalkanes, *Journal of Physical Chemistry A*, 1998, **102**, 5822–5830.